Sub-pixel processing for super-resolution scanning imaging system with fiber bundle coupling

Bowen An (安博文)[1,2*], Bingbin Xue (薛冰玢)[1], Shengda Pan (潘胜达)[2], and Guilin Chen (陈桂林)[2]

[1] *School of Information Engineering, Shanghai Maritime University, Shanghai* 200135*, China*

[2] *Shanghai Institute of Technical Physics, Chinese Academy of Sciences, Shanghai 200083, China*

[*] *Corresponding author: anbowen@sina.com*

Received January 28, 2011; accepted March 15, 2011; posted online June 16, 2011

A multilayer fiber bundle is used to couple the image in a remote sensing imaging system. The object image passes through all layers of the fiber bundle in micro-scanning mode. The malposition of adjacent layers arranged in a hexagonal pattern is at sub-pixel scale. Therefore, sub-pixel processing can be applied to improve the spatial resolution. The images coupled by the adjacent layer fibers are separated, and subsequently, the intermediate image is obtained by histogram matching based on one of the separated image called base image. Finally, the intermediate and base images are processed in the frequency domain. The malposition of the adjacent layer fiber is converted to the phase difference in Fourier transform. Considering the limited sensitivity of the experimental instruments and human sight, the image is set as a band-limited signal and the interpolation function of image fusion is found. The results indicate that a super-resolution image with ultra-high spatial resolution is obtained.

OCIS codes: 100.3008, 100.2000.

doi: 10.3788/COL201109.081001.

Super-resolution has been a hot research area since Tsai *et al.* first proposed the concept in 1984[1]. Generally, the super-resolution inage reconstruction algorithms are classified into two categories: frequency domain processing and space domain processing[2]. However, either processing consists of three phases: registration, interpolation, and restoration. Sub-pixel imaging, closely associcated with super-resolution, is a kind of advanced technology which is widely applied in remote sensing system[3].

Scanning imaging plays a significant role in obtaining high resolution images in remote sensing area. Hence, we propose an imaging system based on fiber coupling, in which a plane-array system was used to receive images. The input structure of fiber is arranged in a hexagonal pilling pattern as shown in Fig. 1. The object image passes through the fiber bundle in all layers while scanning. By fusing the images of different layers, a high resolution image can be obtained. However, the system with the sub-pixel magnitude malposition between adjacent layers in the scanning direction is a sub-pixel imaging system[4]. As to sub-pixel imaging, significant progress has been achieved since SPOT-5 satellite proposed the concept in 2001.

The approach of sub-pixel imaging has been proposed in French SPOT-5. The significant points are the rows of charge-coupled device (CCD) on the focal plane array, which changed from one to two with a malposition of the 0.5 pixel in the linear array direction. This kind of imaging system has two different versions. The spaces between CCD rows in the scanning direction are n (n belongs to natural number) and $n+0.5$ pixels. The horizontal and vertical resolutions of the images obtained by the two versions are the same when the sampling frequency of time in the scanning direction is doubled. The first arrangement is applied in fiber bundle coupling imaging system and spatial resolutions varied with the variation of the time sampling frequency in the scanning direction[5,6].

Sub-pixel imaging multi-sampled the same object in micro-scanning mode, which is scanned at a step of sub-pixel displacement. Suppose d is the distance between fibers, s is the resolution enhancement factor, d/s is the micro-scanning step, and $m \times n$ is the array of the fiber bundle, then the mathematical model of the micro-imaging is

$$B = (b_1, b_2 \cdots b_{kmn})^{\mathrm{T}} = \frac{1}{s^2} \begin{bmatrix} a_{1,1} \ \ldots \ a_{1,s^2mn} \\ \cdot \\ \cdot \\ a_{kmn,1} \ \ldots \ a_{kmn,s^2mn} \end{bmatrix}$$
$$(x_1, x_2, \ldots x_{s^2mn})^{\mathrm{T}} = AX^{\mathrm{T}}, \quad (1)$$

where B is the array of the observed image, X is the array of the object image, and A is the system matrix as decided by the scanning and sampling feature of the detector. If the i-th sensor of the detector contains the j-th pixel of the object image, a_{ij} is defined as 1, otherwise it is 0. Calculating the general inverse of the equation, a higher resolution image, compared with that of one fiber layer coupling system, could be obtained[7]. Therefore, the imaging system was a sub-pixel super-resolution imaging system.

Fusion processing is necessary when the object images are reconstructed due to the fiber bundle arranged in hexagonal mode. The processing consists of preprocessing and fusion.

The uncertain factors during the production of the fiber bundle as well as the non-uniformity of CCD photosensors, causes the transfer function of each fiber to be different from one another. As a result, the intensity of the output image varies under the same illumination condition. Figure 2 shows the actual effects and indicates that the intensities are distinctly different between layers. Hence, it is necessary to calibrate the images coupled by adjacent layers. The related algorithm is shown

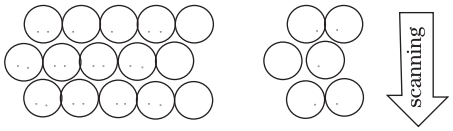

Fig. 1. Input structure of fiber bundle and scanning direction.

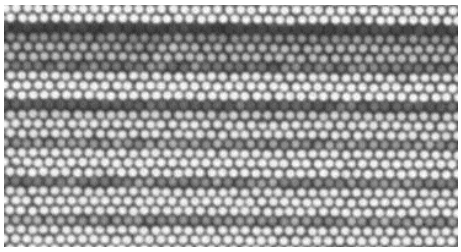

Fig. 2. Different output intensities.

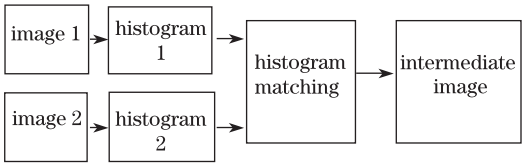

Fig. 3. Histogram matching.

in Fig. 3.

Histogram matching is achieved by specifying the image of one layer as reference. The histogram of the image of the adjacent layer is matched to it.

Set n as the total number of the pixel, n_j as the number of pixel whose gray level is r_j, L as the number of discrete gray level, $P_z(r)$ as the histogram of registration images, $P_r(r)$ as the histogram of images to be matched, and s_k and v_k as variables:

$$s_k = T(r_k) = \sum_{j=0}^{k} p_r(r_j) = \sum_{j=0}^{k} \frac{n_j}{n} k = 0, 1, 2, \cdots, L-1. \tag{2}$$

Suppose there exists a transform function $G(z)$,

$$v_k = G(z_k) = \sum_{j=0}^{k} p_z(z_i) = s_k, \quad k = 0, 1, 2, \cdots, L-1. \tag{3}$$

According to the requirement of calibration,

$$z_k = G^{-1}[T(r_k)] = G^{-1}[(s_k)], \quad k = 0, 1, 2, \cdots, L-1. \tag{4}$$

The intermediate image was generated by histogram matching, which produced the same object with image coupled by specified layer fiber. However, the hexagonal arrangement leads to sub-pixel malposition. Fusing two images for higher spatial resolution became necessary[8−9].

Set '$I_1(x)$' and '$I_2(x)$' as the two images, a as malpositioned space distance, samp (x) as sampling function, and $I(x)$ as the object image.

$$I_1(x) = I(x)\mathrm{samp}(x), \tag{5}$$

$$I_2(x) = I(x)\mathrm{samp}(x + a), \tag{6}$$

$$I(x) = I_1(x) \otimes m_1(x) + I_2(x) \otimes m_2(x), \tag{7}$$

where $\otimes$ represents convolution and $m_i(x)$ represents the interpolation filter[10]. Considering the sensitivity of the experimental instrument and capability of the human sight, the image was set to a band-limited signal and frequency spectrum as

$$F(u) = \begin{cases} F(u) & -\dfrac{1}{p} \leqslant u \leqslant \dfrac{1}{p} \\ 0 & \text{others} \end{cases}, \tag{8}$$

where p is the distance between CCD photosensors.

To solve $m_i(x)$, it is necessary to obtain the Fourier transform values of Eqs. (5) and (6) as

$$F_1(u) = F(u) \times \mathrm{comb}(pu), \tag{9}$$

$$F_2(u) = [F(u) \times \exp(\mathrm{j}2\pi au)]\mathrm{comb}(pu). \tag{10}$$

The two adjacent layers of the fiber have a half-pixel malposition in the scanning direction. Thus, the corresponding amplitude of image frequency spectrum is equal with the different phases.

Considering the constraint condition Eq. (8), spectrum of $I(x)$ was expanded in frequency domain with a period of $1/p$.

$$F_1(u) = \frac{1}{p}\Big[F\Big(u + \frac{1}{p}\Big) + F(u) + F\Big(u - \frac{1}{p}\Big)\Big], \tag{11}$$

$$F_2(u) = \frac{1}{p}\Big\{ \exp\Big[\mathrm{j}2\pi a\Big(u + \frac{1}{p}\Big)\Big]\Big[F\Big(u + \frac{1}{p}\Big) + \exp(\mathrm{j}2\pi au)F(u) + \exp\Big[\mathrm{j}2\pi a\Big(u - \frac{1}{p}\Big)F\Big(u - \frac{1}{p}\Big)\Big]\Big]\Big\}. \tag{12}$$

Using Eqs. (11) and (12):

$$F(u) = -\mathrm{j}\frac{p}{2}\frac{\exp(\mathrm{j}\pi a/p)}{\sin(\pi a/p)}F_1(u) + \mathrm{j}\frac{p}{2}\frac{\exp(-\mathrm{j}\pi a/p)}{\sin(\pi a/p)}\exp(-\mathrm{j}2\pi a)F_2(u). \tag{13}$$

From Eqs. (7), (13), and the principle of sampling:

$$F(u) = F_1(u)M(u) + F_2(u)M(u)\exp(-\mathrm{j}2\pi au), \tag{14}$$

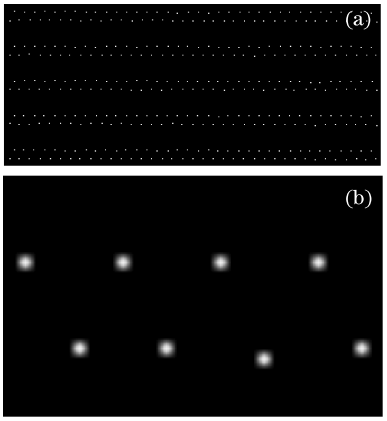

Fig. 4. Positions of adjacent layers. (a) the 2nd and 3rd layers' positions; (b) magnified image.

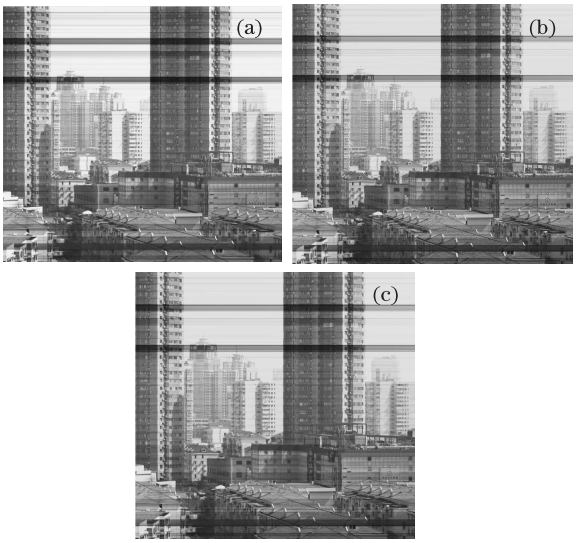

Fig. 5. Images generated by two adjacent layers and the result after histogram matching. (a) The 2nd layer; (b) the 3rd layer; (c) the 3rd layer after histogram matching.

$$M(u) = \frac{p}{2}\mathrm{rect}(\frac{u}{2/p}) - \frac{\mathrm{j}}{2}\mathrm{ctan}\Big(\pi\frac{a}{p}\Big)\mathrm{tri}'\Big(\frac{u}{1/p}\Big). \quad (15)$$

The interpolation filter $m_i(x)$:

$$m_1(x) = m(x) = \mathrm{sinc}\Big(\frac{2}{p}x\Big) - x\frac{\pi}{p}\mathrm{ctan}\Big(\pi\frac{a}{p}\Big)\,\mathrm{sinc}^2\Big(\frac{x}{p}\Big), \quad (16)$$

$$m_2(x) = \ m(a-x) = \mathrm{sinc}\Big[\frac{2}{p}(a-x)\Big] - (a-x)\frac{\pi}{p} \mathrm{ctan}\Big(\tau\frac{a}{p}\Big)\,\mathrm{sinc}^2\Big(\frac{a-x}{p}\Big). \quad (17)$$

Hexagonal arrangement was adopted in producing fiber bundle and the size of the malposition between adjacent fibers was $a/2$. Thus,

$$m(x) = \mathrm{sinc}\Big(\frac{2}{p}x\Big). \quad (18)$$

The $m(x)$ in Eqs. (16) and (17) can be substituted by Eq. (18), and the fused image is obtained using Eq. (7).

Adhering to the abovementioned theories, microscanning was carried out and the obtained images were processed subsequently. There were four fiber layers in the input terminal of the coupling bundle. The position of each fiber was located accurately based on previous studies[11]. The second and third layers are shown in Fig. 4. Malposition of the adjacent fiber layers was obvious at half-pixel scale, particularly in the magnified image.

The step number of the half-cycle was set to 8 000 in the scanning experiment and the step length was set to ensure that the same location of the image of the object would pass through adjacent layers by turn. The number of fibers in one layer was approximately 7 500. The imaging targets were buildings approximately 1 km away. Therefore, the image size was 7 500 × 8 000 pixels without super-resolution processing, whereas it was 15 000×16 000 pixels after processing.

Figures 5(a) and (b) show the coupling image of the second and third layers, respectively. The histogram of the image in the 3rd layer was matched based on the histogram of the 2nd layer[12]. Figure 5(c) shows the result. The histograms of the three images are shown in Fig. 6. Figure 7 was generated by fusing Figs. 5(a) and (c)[13], and shows further details of the object.

The size of the Fig. 7 was exceedingly large that it can only be partly shown in a different scale on the computer using the software ACDSee. Figures 8(a) and (b) in 30%, 50% proportions, respectively, show the part corresponding to the lower right corner of the image containing Chinese characters. During the imaging, a single-lens reflex camera, 12.3 million pixels (D90, Nikon, Japan), was used to obtain the image in the same position of the same target. Figure 8(c), which is in 100% proportion, shows the same content. Comparing these images facilitated the conclusion that the spatial resolution of the fiber bundle coupling imaging system was ultra high.

Due to the limitations of the manufacturing technology, ensuring that each fiber input plane was perpendicular to the bundle direction was difficult. When the obliquity reached a certain degree, the transfer function of the system decreased significantly, causing the appearance of the shadow belts in Figs. 6–8. When the imaging target was a white screen of a liquid crystal display (LCD) display, it was surprising to discover that the imaging system could distinguish between the three primary colors red, green, and blue of each physical pixel. The details are shown in the Fig. 9.

In conclusion, the scanning imaging with image carrying fiber bundle coupling is an innovative approach.

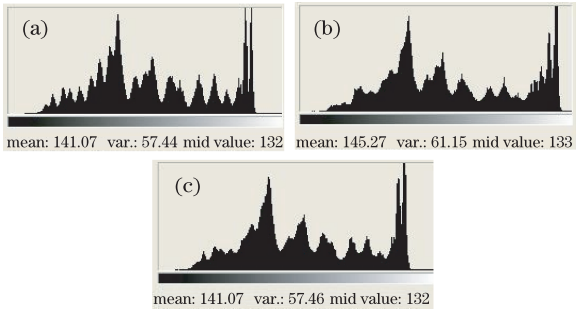

Fig. 6. Histogram of (a) the 2nd layer; (b) the 3rd layer; and (c) the 3rd layer after histogram matching.

Fig. 7. Image after fusion.

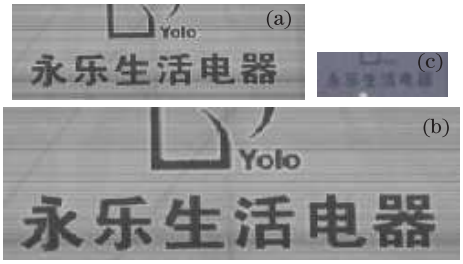

Fig. 8. Different scaling images and the comparison. (a) In 30% scaling; (b) in 50% scaling; (c) the comparison: Nikon in 100%.

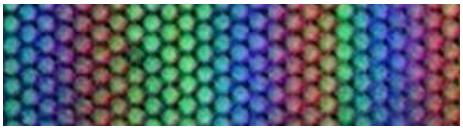

Fig. 9. Primary colors of the LCD physical pixel.

Focusing on the hexagonal structure of the fiber bundle, micro-scanning is conducted to ensure that the same part of the object image passes through the adjacent layers. Histogram matching and image fusion are introduced into sub-pixel processing. The results indicate an ultra-high spatial resolution of the super-resolution imaging system.

This work was supported by the National High Technology Research and Development Program of China (No. 2007AA12Z152), the Innovation Foundation of Shanghai Education Bureau, the Foundation of Shanghai Shuguang Project (No. 2008SG49), the Shanghai Natural Science Foundation (No. 11ZR1415200), and the Leading Academic Discipline Project of Shanghai Municipal Education Commission (No. J50602). The authors also acknowledge the help of the Shanghai Maritime University and Shanghai Institute of Technical Physics.

References

1. R. Y. TSai and T. S. Huang, IEEE Trans. Acoust. Speech Signal Process. **Assp 31,** 213 (1984).
2. S. Xiao, G. Han, and Y. Wo, J. Comp. Sci. (in Chinese) **36,** 8 (2009).
3. R. Song, "Research on super resolution reconstruction" (in Chinese), PhD. Thesis (Xidian University, 2009).
4. J. Cao, " Research on image superresolution processing, superresolution imaging and their correlative technologies" (in Chinese), PhD. Thesis (National University of Defense Technology, 2004).
5. X. Sui, Q. Chen, and H. Lu, J. Infrared Millim. Waves (in Chinese) **26,** 377 (2007).
6. W. Jin, C. Wang, N. Zhang, L. Wamg, and P. Lu, J. Infrared Millim.Waves (in Chinese) **24,** 261 (2005).
7. Y. Chen, W. Jin, L. Wang, and X. Wang, Chin. Opt. Lett. **8,** 146 (2010).
8. H. Li, S. Xu, and D. Yan, Laser Technol. (in Chinese) **32,** 493 (2008).
9. Y. Liu, X. Zhang, and J. Zhang, Chin. J. Opt. Appl. Opt. (in Chinese) **2,** 102 (2009).
10. W. Liu, J. Cui, and L. Zhou, J. Computer-Aided Design & Computer Graphics (in Chinese) **19,** 1273 (2005).
11. B. An, S. Pan, and G. Chen, J. Infrared Millim. Waves (in Chinese) **29,** 156 (2010).
12. W. Yan, Z. Tian, L. Pan, and M. Ding, Chin. Opt. Lett. **7,** 201 (2009).
13. Q. Guo and S. Liu, Chin. Opt. Lett. **8,** 656 (2010).